

## V–I characteristics of solid polymer electrolytic (SPE) dehumidifier

Shuichi Sakuma · Shiro Yamauchi ·  
Osamu Takai

Received: 19 September 2010 / Accepted: 25 March 2011 / Published online: 9 April 2011  
© Springer Science+Business Media B.V. 2011

**Abstract** Measurements of the V–I characteristics of a solid polymer electrolytic (SPE) dehumidifier were done using a modified SPE dehumidifier with four electrodes which included two electrodes to carry the main current and the other two electrodes to measure the voltages applied to the electrical double layer, which are the boundary voltages between the electrodes and the SPE membrane. The measured results were analyzed using the Butler–Volmer equation to examine the validity of the measurements. The current flowing in the dehumidifier is produced by the decomposition of water near the anode. Therefore, under a steady-state condition, the current should be proportional to the supply rate of water to the anode. On the other hand, a two-layer model for the SPE dehumidifier presented in our previous article showed that the current flowing in the dehumidifier was roughly proportional to the water content in the vicinity of the anode. These results were introduced for interpretation of the V–I measurements of the SPE dehumidifier. It was concluded that the dehumidifier current was expressed in the form of a Butler–Volmer equation as a function of the electrode boundary voltages which were the voltages across the boundary between the electrodes and the SPE membrane.

An experimental formula for the current under a steady-state condition was developed as a function of the water content near the anode and the boundary voltages.

**Keywords** Electrolysis · Dehumidifier · V–I characteristics · Solid polymer electrolytic membrane

### List of symbols

#### Variables

$A$	Area of the dehumidifying element ( $\text{cm}^2$ )
$B$	Coefficient of rate constant ( $\text{cm s}^{-1}$ )
$C_a(T)$	Coefficient to give steady-state current ( $\text{A cm g}^{-1}$ )
$C_I(T)$	Coefficient to give steady-state current ( $\text{A cm g}^{-1}$ )
$c_R$	Molar concentration of reductant ( $\text{mol cm}^{-3}$ )
$c_O$	Molar concentration of oxidant ( $\text{mol cm}^{-3}$ )
$D$	Diffusion coefficient of water in the dehumidifying element ( $\text{cm}^2 \text{s}^{-1}$ )
$E_{0,a}$	The voltage across the anode-side boundary when the current is zero (V)
$E_a$	Electrical potential of anode (V)
$E_c$	Electrical potential of cathode (V)
$E_m$	Electrical potential of electrode (V)
$E_s$	Electrical potential of solid polymer electrolytic membrane (V)
$E_{sa}$	Electrical potential of the anode-side end of SPE membrane (V)
$E_{sc}$	Electrical potential of the cathode-side end of SPE membrane (V)
$F$	Faraday constant (=96,440 Coulombs)
$I$	Current of the dehumidifying element (A)
$I_a, I_c$	Anode current and cathode current, respectively (A)

S. Sakuma (✉)  
Ryosai Technica Co., Ltd, 8-1-1, Tsukaguchi-Honmachi,  
Amagasaki, Hyogo 661-0001, Japan  
e-mail: Sakuma.Shuichi@ryosai.co.jp

S. Yamauchi  
Tada Electric Co., Ltd, 488, Shimokasaka, Oku-cho,  
Setouchi 701-4247, Japan

O. Takai  
Nagoya University, Furocho, Chikusa-ku,  
Nagoya 464-8603, Japan

$I_{st}$	Steady-state current (A)
$I_{sat}$	Saturated current (A)
$k$	Rate constant of oxidation or reduction (cm s <sup>-1</sup> )
$k_{a,+}, k_{a,-}$	Rate constants of oxidation and reduction at the anode-side double layer (cm s <sup>-1</sup> )
$k_{c,+}, k_{c,-}$	Rate constants of oxidation and reduction at the cathode-side double layer (cm s <sup>-1</sup> )
$L$	Thickness of the dehumidifying element (cm)
RH	Relative humidity (%)
$R$	Gas constant (=8.31 J mol <sup>-1</sup> K <sup>-1</sup> )
$R_s$	Electrical resistance of the dehumidifying element ( $\Omega$ )
$T$	Temperature of the air space surrounding the dehumidifying element (K)
$\beta_a, \beta_c$	Transfer coefficients defined for anode-side boundary and cathode-side boundary, respectively
$\Delta^*G$	Gibbs activation energy (J mol <sup>-1</sup> )
$\Delta\phi_m^o$	Standard electrode potential when all chemical materials have activity values of 1 (V)
$\kappa_g$	Coefficient relevant to the diffusion velocity of water from the air to the SPE membrane (cm s <sup>-1</sup> )
$\kappa_s$	Coefficient relevant to the diffusion velocity of water from the membrane to the air (cm s <sup>-1</sup> )
$\rho_g$	Water density in the air surrounding the dehumidifying element (g cm <sup>-3</sup> )
$\rho_{s,a}, \rho_{s,c}$	Water contents in the vicinity of the anode and in the vicinity of the cathode of the dehumidifying element (g cm <sup>-3</sup> )
$\rho_{s,o}$	Water content of the dehumidifying element in equilibrium with environmental humidity (g cm <sup>-3</sup> )

## Subscripts

- a Positive electrode or anode
- c Negative electrode or cathode
- g Gas space
- s Solid polymer electrolytic dehumidifying element
- +
- Reduction

## 1 Introduction

The authors have developed an electrolytic dehumidifying device using a solid polymer electrolyte membrane (SPE membrane) as a protective measure against problems caused by high humidity. The dehumidifying device was found to effectively maintain highly reliable electrical and electronic devices by controlling the humidity in the space containing them. This type of electrolytic dehumidifying

device has several advantages of no-drain, space-saving and small input-power compared to conventional dehumidifying techniques such as those using a Peltier element or a space heater.

The dehumidifying processes of the dehumidifying device can be well simulated by a two-layer model for the dehumidifying device that was proposed in our previous article [1, 2], and it was also shown [2] that the current flowing in the device was proportional to the water content in the vicinity of the anode when the applied voltage was constant.

In this article, an experiment involving the V-I characteristics of the dehumidifying device is presented. The experiment was done using a modified dehumidifying device, which contained two reference-electrodes in order to measure the electrode-membrane voltages, in addition to the normal electrodes carrying the main current. The V-I characteristics were analyzed using the water content at the anode introduced in our previous article and estimated by comparison with the Butler-Volmer equation. The dependences of the current on the anode and cathode voltages were experimentally obtained. The voltage supported by the SPE membrane itself was also estimated from the voltage difference between the reference electrodes.

These results will be useful in understanding what kind of reaction determines the rate of reaction.

## 2 Operating principle of SPE dehumidifying device

### 2.1 Relation of overvoltage and current

The principle of dehumidification by the SPE dehumidifier is shown in Fig. 1. The electrode reactions at the anode and the cathode are given by the following formulas.

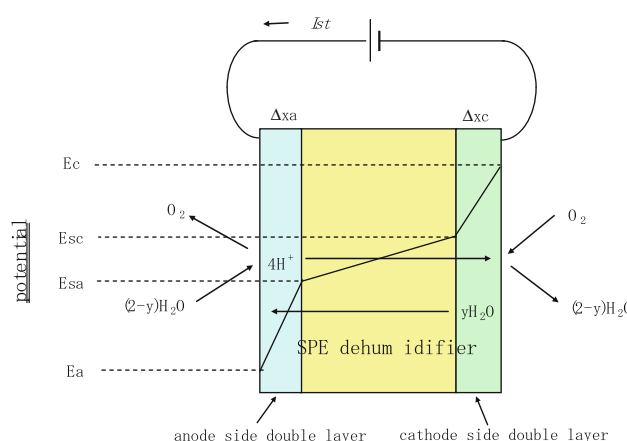
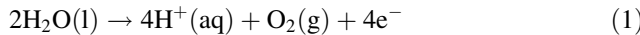
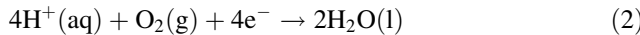


**Fig. 1** Principle and water flow of SPE dehumidifying element and electrical potentials at the anode-side boundary, cathode-side boundary and membrane bulk

At the anode,



At the cathode,



Water molecules near the anode in the dehumidifying element are decomposed into protons and oxygen. The protons drift to the cathode and combine with oxygen to form water near the cathode. The electrolysis of water and the recombination of protons and oxygen occur at the boundary between the electrodes and the membrane. At the anode, water is supplied from the space facing the anode and from the cathode by diffusion. The anode-side boundary and cathode-side boundary are denoted as the anode-side double layer and cathode-side double layer, respectively. The electrolysis and the recombination of water are performed based on the voltage differences across each double layer. The current produced by the decomposition of water molecules at the anode must be proportional to the supply rate of water molecules to the anode under a steady-state condition.

When no current flows in the element, the anode and cathode are in equilibrium with the SPE membrane to form electrical double layers near the electrodes. These electrical double layers produce electrical potential differences between the electrodes and the membrane. The potential difference between the electrodes and SPE membrane are given by the Nernst equation as follows.

$$E_m - E_s = \Delta\phi_m^o - \frac{RT}{4F} \ln \frac{a_{\text{H}_2\text{O}}^2}{a_{\text{H}^+}^4 a_{\text{O}_2}^2} \quad (3)$$

where,  $E_m$  and  $E_s$  are the electrical potentials of the electrode and membrane.  $\Delta\phi_m^o$  is the standard electrode potential, and it denotes the electrical potential of the electrode to the SPE membrane when all the chemical materials have activity values of 1. This electrode potential relative to the SPE membrane cannot be measured in principle. The electrode potential is usually given and measured by a potential difference relative to a standard electrode such as a standard hydrogen electrode. However, the changes in the potential across the double layer can be measured if the polarization or its change created at a reference electrode used to measure the potential change is small.

On the other hand, when current flows in the dehumidifying element, the current can be expressed as follows.

At the anode,

$$I_a = FA(k_{a,+}c_R - k_{a,-}c_O) \quad (4)$$

At the cathode,

$$I_c = FA(k_{c,-}c_O - k_{c,+}c_R) \quad (5)$$

where  $F$  and  $A$  are the Faraday constant and the dehumidifying area of the element, respectively. The

values of  $k_{a,+}$ ,  $k_{a,-}$  and  $k_{c,+}$ ,  $k_{c,-}$  are the rate constants of the oxidation and reduction at the anode-side double layer and those at the cathode-side double layer, respectively. The values of  $c_O$  and  $c_R$  are the molar concentrations of the oxidant and reductant in the reaction, respectively.

The rate constants can be expressed as follows [3].

$$k = B \exp(-\Delta^*G/RT) \quad (6)$$

where  $\Delta^*G$  and  $B$  are the Gibbs activation energy and a coefficient with the same dimension as the rate constant, respectively. Substituting Eq. 6 into Eq. 4, the following equation is obtained.

$$I_a = FA \{ B_{a,+}c_R \exp(-\Delta^*G_a/RT) - B_{a,-}c_O \exp(-\Delta^*G_c/RT) \} \quad (7)$$

The Gibbs activation energy in Eq. 7 is given for the voltage difference  $\varphi_m$  across the electrical double layer as follows [3].

$$\begin{aligned} \Delta^*G_c &= \Delta^*G_c(0) + \beta F \Delta\phi_m \\ \Delta^*G_a &= \Delta^*G_a(0) - (1 - \beta) F \Delta\phi_m \end{aligned} \quad (8)$$

Substituting Eq. 8 into 7, the following equation is obtained.

$$\begin{aligned} I_a &= F A B_{a,+} c_R \exp(-\Delta^*G_a(0)/RT) \exp\{(1 - \beta_a) F \Delta\phi_m/RT\} \\ &\quad - F A B_{a,-} c_O \exp(-\Delta^*G_c(0)/RT) \exp\{-\beta_a F \Delta\phi_m/RT\} \end{aligned} \quad (9)$$

$\beta_a$  is the transfer coefficient at the anode.

The following Butler–Volmer equation is obtained assuming that  $\Delta\phi_m = E_{0,a}$ , when  $I_a = 0$ ,

$$\begin{aligned} I_a &= i_{0,a} \exp\{(1 - \beta_a) F(E_a - E_{sa} - E_{0,a})/RT\} \\ &\quad - i_{0,a} \exp\{-\beta_a F(E_a - E_{sa} - E_{0,a})/RT\} \end{aligned} \quad (10)$$

Here,

$$\begin{aligned} i_{0,a} &= F A B_{a,+} c_R \exp(-\Delta^*G_a(0)/RT) \exp\{(1 - \beta_a) F E_{0,a}/RT\} \\ &= F A B_{a,-} c_O \exp(-\Delta^*G_c(0)/RT) \exp\{-\beta_a F E_{0,a}/RT\} \end{aligned} \quad (11)$$

On the other hand, the current at the cathode can be described as follows by applying a procedure similar to that already described.

$$\begin{aligned} I_c &= i_{0,c} \exp\{\beta_c F(E_{sc} - E_c - E_{0,c})/RT\} \\ &\quad - i_{0,c} \exp\{-(1 - \beta_c) F(E_{sc} - E_c - E_{0,c})/RT\} \end{aligned} \quad (12)$$

where  $\beta_c$  is the transfer coefficient at the cathode.

Under a steady-state condition,

$$I_a = I_c \equiv I_{st} \quad (13)$$

As shown in Eqs. 10 and 12, these currents flowing in devices such as the SPE dehumidifier are expected to

depend on the exponent of the potential difference across the double layers.

## 2.2 Consideration of the steady-state current and effect of the water concentration on the current

The current flowing in the dehumidifying element is produced in the anode-side double layer by the decomposition of water molecules. Therefore, the current under a steady-state condition should be proportional to the supply rate of water to the anode area. The authors showed the relation between the steady-state current of the dehumidifying element and the water content in the vicinity of the electrodes in a previous article [2], as follows.

$$I_{st} = C'(T) \left\{ A(\kappa_g \rho_g - \kappa_s \rho_{s,a}) + \frac{DA(\rho_{s,c} - \rho_{s,a})}{L} \right\} \quad (14)$$

$$I_{st} = C'(T) \left\{ A(\kappa_s \rho_{s,c} - \kappa_g \rho_g) + \frac{DA(\rho_{s,c} - \rho_{s,a})}{L} \right\} \quad (15)$$

where,  $\rho_{s,a}$  and  $\rho_{s,c}$  are the water contents in the vicinity of the anode and cathode of the element, respectively.  $\rho_g$  is the water density of the space surrounding the element. The first and second terms on the right side of Eq. 14 are the water supply rates to the anode area from the space facing the anode and from the cathode by diffusion, respectively. In Eq. 15, the first and second terms on the right side are the water rate emitted from the cathode area to the space facing the cathode and to the anode through the element by diffusion, respectively. The water content of the element under an equilibrium condition ( $I_{st} = 0$ ) is denoted as  $\rho_{so}$  and the following quantity of  $\Delta\rho_s$  is introduced.

$$\kappa_s \rho_{so} = \kappa_g \rho_g \quad (16)$$

$$\rho_{s,a} = \rho_{so} - \Delta\rho_s \quad (17)$$

Equations 14 and 15 can be transformed using Eqs. 16 and 17 as follows.

$$I_{st} = C'(T)A \left( \kappa_s + \frac{2D}{L} \right) \Delta\rho_s \equiv C_1(T)A \Delta\rho_s \quad (18)$$

The coefficient of  $C_1(T)$  can be estimated by the following equation, because the current should have a saturated value of  $I_{sat}$ , when the supply rate of water to the anode has a maximum value, that is,  $\Delta\rho_s$  is nearly equal to  $\rho_{so}$ . Assuming that the maximum water supply rate is realized when  $\Delta\rho_s = \rho_{so}$

$$C_1(T) = I_{sat}/(A \rho_{so}) \quad (19)$$

From Eqs. 17, 18, and 19, the following equation is obtained.

$$\begin{aligned} \rho_{s,a} &= \rho_{s,o}(1 - I_{st}/I_{sat}) \\ \rho_{s,c} &= \rho_{s,o}(1 + I_{st}/I_{sat}) \end{aligned} \quad (20)$$

On the other hand, the current of the SPE dehumidifying element was found to be proportional to the water content in the vicinity of the anode, and the following formula was presented in our previous article [1, 2], when the applied voltage is constant.

$$I_{st} = C_a(T)A \rho_{s,a} \quad (21)$$

This equation can be expanded to the following formula for application when the applied voltage is changed.

$$I_{st} = C'_a(T)A \rho_{s,a} f(E_a - E_{s,a}) \quad (22)$$

By substituting Eq. 20 into 22, the following formula is obtained.

$$f(E_a - E_{s,a}) = \frac{1}{C_a(T)A \rho_{s,o}} \frac{I_{st}}{(1 - I_{st}/I_{sat})} \quad (23)$$

Because the cathode current flows by the reduction of protons at the cathode to form water, the relation of the cathode current and the density of protons at the cathode may be expressed as follows.

$$I_{st} = C_c(T)A_c [H^+] g(E_{sc} - E_c) \quad (24)$$

where  $[H^+]$  is the concentration of protons at the cathode. However, the information on the concentration of protons at the cathode is still unknown. Therefore, the relation of the cathode current and the cathode-side boundary voltage will be shown as the current versus the boundary voltage by a Tafel plot.

The feature of  $f(E_a - E_{s,a})$  and  $g(E_{sc} - E_c)$  can be obtained from the data for the V-I measurements by graphical representation of  $I_{st}/(1 - I_{st}/I_{sat})$  vs.  $V_{a,sa}$ . Also,  $I_{st}$  vs.  $V_{sc,c}$ .

## 3 Experiments

The experimental set-up for the V-I measurements of the SPE dehumidifying element is shown in Fig. 2. The tested element has four electrodes, two normal electrodes carrying the main current and two reference electrodes used to measure the potential difference between the anode and membrane or the cathode and membrane. The main electrodes carrying the main current have a larger area of about 70 mm × 70 mm square, each with a hole of 15 mm × 15 mm in their centers. The two reference electrodes with a smaller area of 10 mm × 10 mm square are positioned in the center holes of the larger electrodes. The main current flows across the larger electrodes, and the reference electrodes with smaller areas are used to measure the voltage change

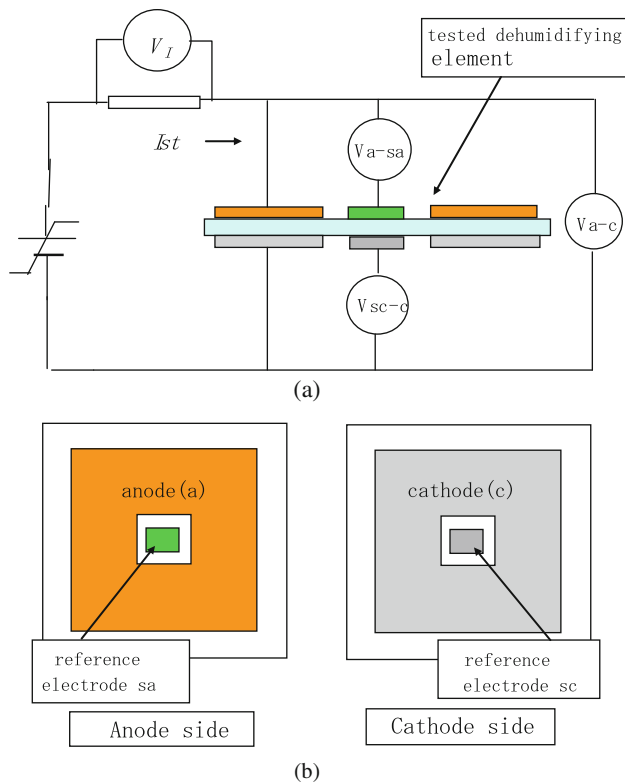


**Fig. 2** Test circuit and test dehumidifying element for V-I measurements of SPE dehumidifier. **a** Test circuit for V-I measurements. **b** Tested SPE dehumidifying element with four electrodes

between the main current electrodes and the membrane. The measured voltages are denoted as  $V_{a,c}$ , the applied voltage between the anode and cathode,  $V_{a,sa}$ , the anode-side boundary voltage between the anode and anode-side reference electrode, and  $V_{sc,c}$ , the cathode-side boundary voltage between the cathode-side reference electrode and the cathode. The V-I measurements were carried out by stepwise varying the applied voltage. Such a test element with a reference electrode to measure the voltage difference as well as a pair of main electrodes carrying the main current was described by Yamauchi et al. [4].

Two tested elements were used for this experiment. They are referred to as sample A and sample B. The tested elements are composed of a Nafion 117 membrane with four electrodes on both of its surfaces. The four electrodes are made of porous electrodes and a catalyst mainly composed of platinum black.

The element was placed in an open box in order to avoid an effect by forced convection from its surrounding environment. The element with the open box was placed in a vessel in order to control the temperature and humidity.

Figure 3 shows typical data obtained by V-I measurements of sample A under the conditions of 313 K and 60%. The current does not increase with an increase in the applied voltage in its smaller region, but the current linearly

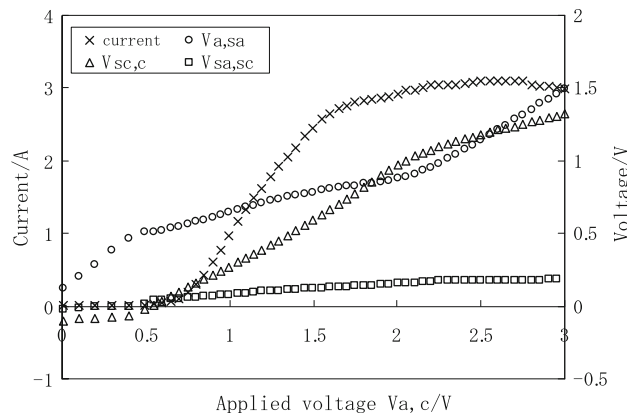


**Fig. 3** V-I measurements for the temperature and humidity of 313 K, 60% (sample A)

increased in the middle region of the applied voltage. In the higher voltage range, the current becomes saturated. The saturated value seems to be a reflection of the rate-determining step. The anode-side boundary voltage of  $V_{a,sa}$  increases at a rate similar to the increase in the applied voltage in the lower applied voltage range. The increasing rate of the voltage then decreases in the middle range of the applied voltage, and in the higher range, the increasing rate of the voltage increases again. The increasing rate of the anode-side boundary voltage is the lowest in the range where the increasing current rate is the highest. Thus, the anode-side boundary voltage quite effectively causes a current increase.

The voltage of  $V_{sc,c}$  does not increase with an increase in the applied voltage in the lower range. The voltage is then increased, linearly synchronized with the current increase in the middle applied voltage range, and in the higher range, the voltage increase rate is reduced. The increasing rate of the cathode-side boundary voltage is the highest in the range when the increasing current rate is the highest. The cathode-side boundary voltage seems to be mainly proportional to the current or the supply rate of protons to the cathode.

The voltage, denoted by  $V_{sa,sc}$ , is the difference in  $V_{a,c}$  and ( $V_{a,sa} + V_{sc,c}$ ) and will be the voltage across the membrane itself. The voltage  $V_{sa,sc}$  increased very slowly with the current increase.

These phenomena seem to be classified into the following three ranges,

- (1) The range of a low applied voltage where no current flows and most of the applied voltage is related to the anode-side boundary voltage  $V_{a,sa}$ .
- (2) The middle range where the current is increased with the applied voltage and the increasing rate of cathode-side boundary voltage is greater than that of the anode-side boundary voltage
- (3) The higher applied voltage range in which the current is saturated.

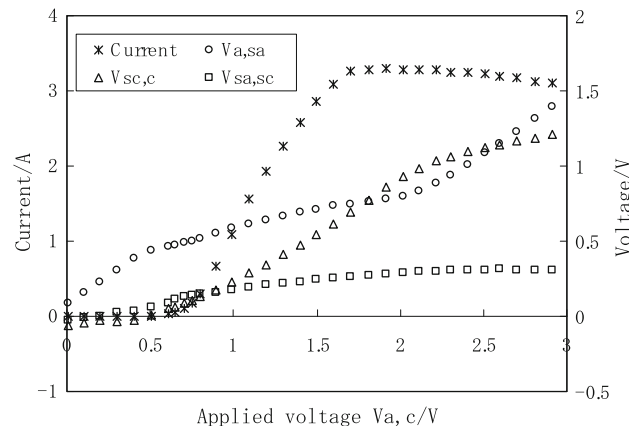
Figures 4 and 5 are the V–I measurements of sample A under the conditions of 303 K/60% and 293 K/60%, respectively. These figures show that the V–I characteristics are similar to those at 313 K/60% shown in Fig. 3.

Figures 6, 7, and 8 are the V–I measurements of sample B for the different humidities of 80, 60, and 30%, respectively. These figures also show the V–I characteristics similar to those of Fig. 3, 4, and 5.

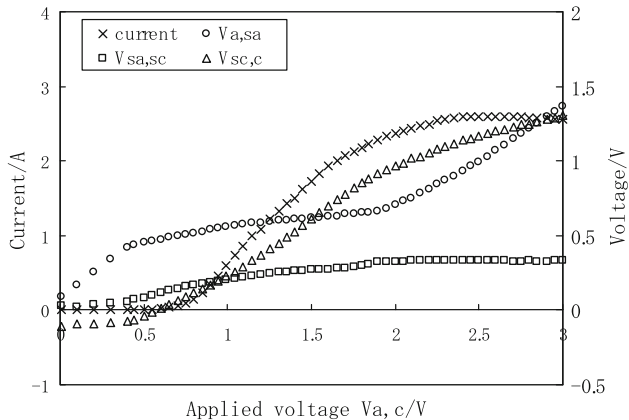
These V–I data shown in Figs. 3, 4, 5, 6, 7, and 8 are processed into the form shown in Figs. 9 and 10 to estimate  $f(V_{a,sa})$  and  $g(V_{sc,c})$  which are expressed by Eq. 23 and 24, respectively.

Figure 9 shows the current characteristics for different temperatures ranging from 293 K to 313 K, obtained from the experiment using sample A. Figure 9a shows the current characteristics for the anode-side boundary voltage,  $V_{a,sa}$ . The figure is represented in the form of  $I_{st}/(1 - I_{st}/I_{sat})$  versus  $V_{a,sa}$ . It was found from the figure that these currents begin to increase at  $V_{a,sa}$  equals 0.4 volt or more, and the

gradients of the currents for the anode-side boundary voltage in its lower region are about 34, 38 and 41 V<sup>-1</sup> for the temperatures and humidities of 313 K/60%, 303 K/60% and 293 K/60%, respectively. The gradients decrease to some



**Fig. 6** V–I measurements for the temperature and humidity of 303 K, 80% (sample B)



**Fig. 4** V–I measurements for the temperature and humidity of 303 K, 60% (sample A)

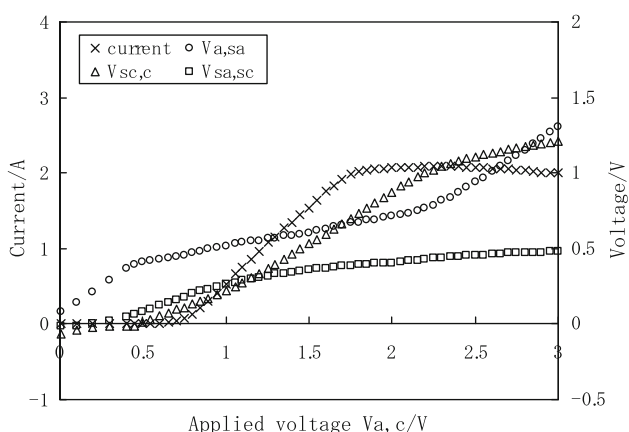


**Fig. 5** V–I measurements for the temperature and humidity of 293 K, 60% (sample A)

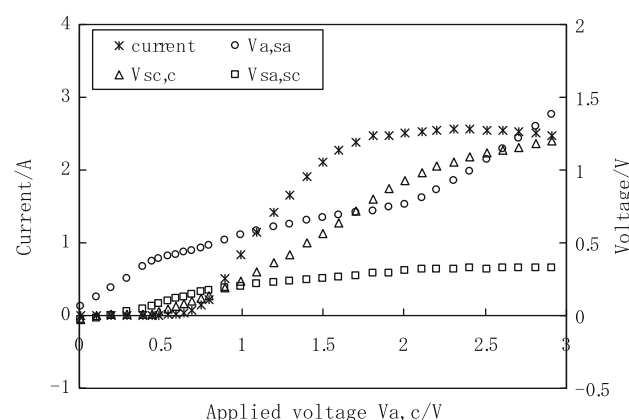


**Fig. 7** V–I measurements for the temperature and humidity of 303 K, 60% (sample B)

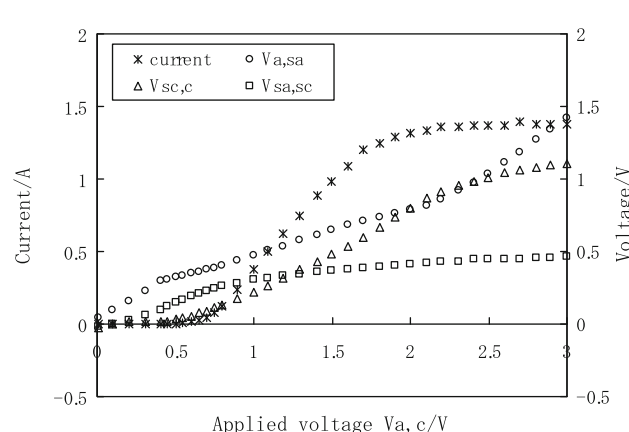
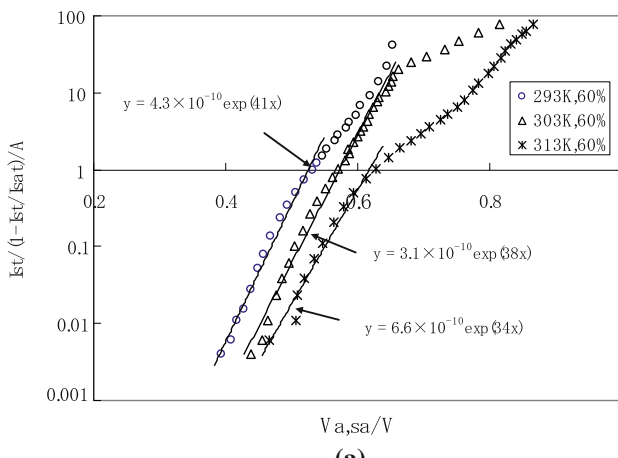
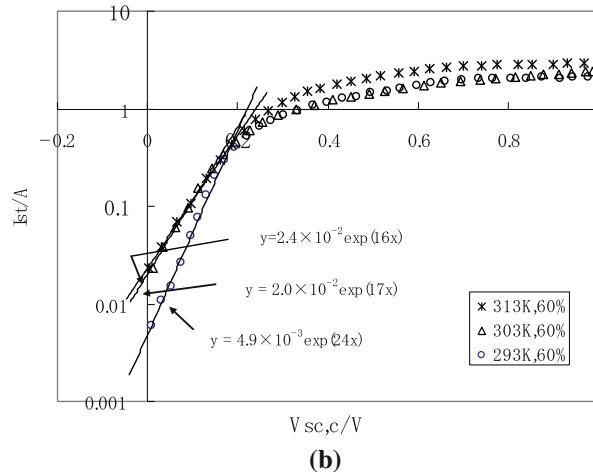


**Fig. 8** V–I measurements for the temperature and humidity of 303 K, 30% (sample B)



(a)

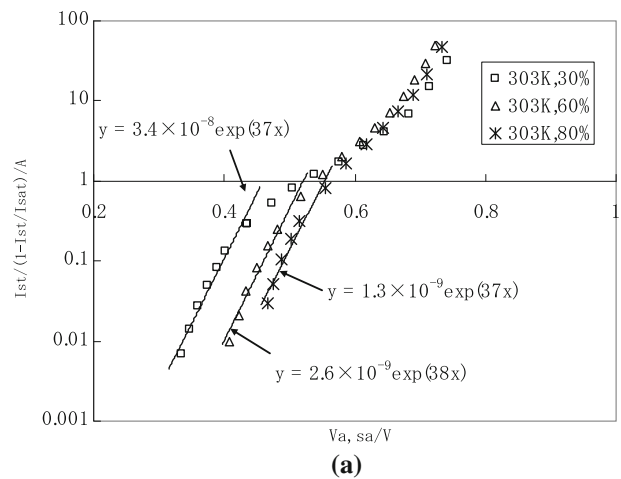


(b)

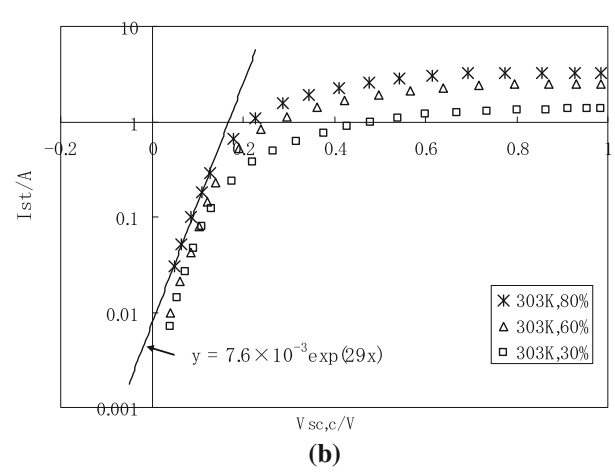
**Fig. 9** Current versus anode-side boundary voltage and cathode-side boundary voltage for different temperatures (sample A). **a** Current versus anode-side boundary voltage  $V_{a,sa}$  for different temperatures. **b** Current versus cathode-side boundary voltage  $V_{sc,c}$  for different temperatures

degree in the larger anode-side boundary voltage when the current  $I_{st}$  approaches  $I_{sat}$ . Figure 9b shows the current characteristics for the cathode-side boundary voltage,  $V_{sc,c}$ . As shown in Fig. 9b, the currents increase at a voltage lower than about 0.3 V, at the rate of about 16, 17, and 24  $\text{V}^{-1}$  at 313, 303, and 293 K, respectively. The rate is nearly half compared to that shown in Fig. 9a. The current characteristics for the cathode-side boundary voltage are saturated at the voltages greater than 0.7 V.

Figure 10 shows the current characteristics for the temperature of 303 K and different humidities ranging from 30 to 80%. These data were obtained from the experiment using sample B. The current characteristics for the anode-side boundary voltage are shown in Fig. 10a. The currents were expressed in the form of  $I_{st}/(1 - I_{st}/I_{sat})$ . The currents increase at around  $V_{a,sa}$  equals 0.4 V or more,



(a)



(b)

**Fig. 10** Current versus anode-side boundary voltage and cathode-side boundary voltage for different humidities (sample B). **a** Current versus anode-side boundary voltage  $V_{a,sa}$  for different humidities. **b** Current versus cathode-side boundary voltage  $V_{sc,c}$  for different humidities

at the increasing rate similar to each other and to the one shown in Fig. 9a. Figure 10b shows the current versus cathode-side boundary voltage. The increasing rates of these currents are similar to each other and are about 29  $\text{V}^{-1}$  for voltages less than 0.2 V. This value is greater than the one shown in Fig. 9b.

The results obtained by this experiment are summarized in Table 1. As seen in Table 1, the current gradient for the anode-side boundary voltage is found to be  $F/RT$  for each case.

These characteristics can be expressed in the following form.

$$I_{st} = C_a * (T) A \rho_{s,a} \exp\left(\frac{F V_{a,sa}}{RT}\right) \quad (25)$$

At the cathode, the gradient of the current for cathode-side boundary voltage is about  $F/2RT$  to  $F/1.4RT$  in the

**Table 1** Characteristic electrical values of SPE dehumidifying element

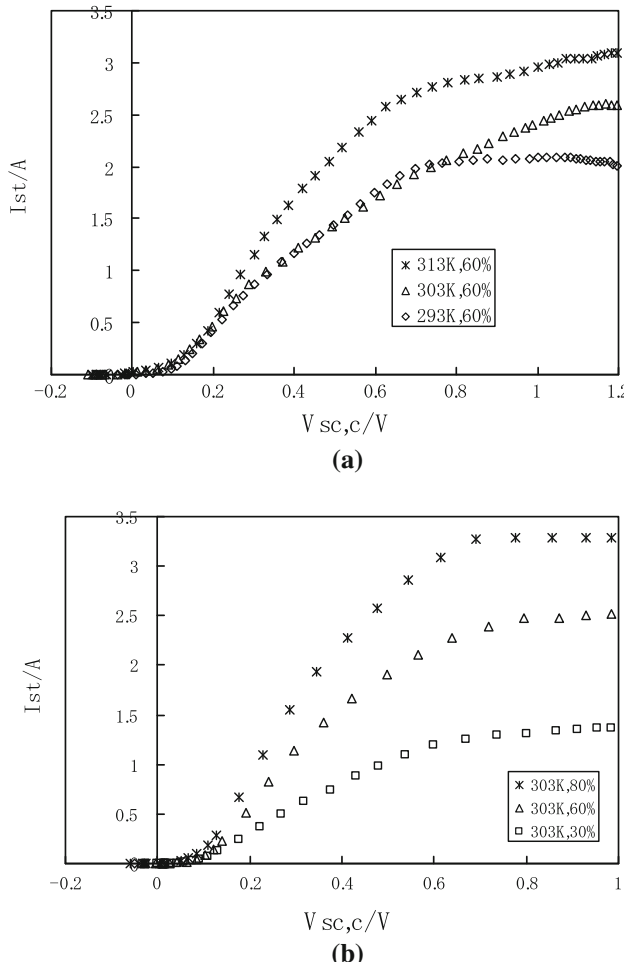
Temperature, $T$ (K)	Relative humidity, RH (%)	Water content, $\lambda$ $\text{H}_2\text{O}/\text{SO}_3\text{H}$	$F/RT$ (V $^{-1}$ )	$(1 - \beta_a) F/RT$ (V $^{-1}$ )	$\beta_c F/RT$ (V $^{-1}$ )	Resistance of membrane (RM $\Omega$ )	Conductivity of membrane ( $\sigma/\text{S cm}^{-1}$ )	Remarks
293	60	About 4	39.6	41	22	0.097	0.0021	Sample A
303			38.3	38	19	0.065	0.0032	
313			37.1	34	16	0.030	0.0069	
303	80	About 5	38.3	37	29	0.036	0.0058	Sample B
303	60	About 4	38.3	38	31	0.044	0.0047	
303	30	About 2	38.3	37	34	0.11	0.0019	

voltage range of less than about 0.3 V, and the characteristics can be expressed in the following form.

$$I_{st} = C_c * (T) A_c \exp\left(\frac{FV_{sc,c}}{(1.4 \sim 2)RT}\right) \quad (26)$$

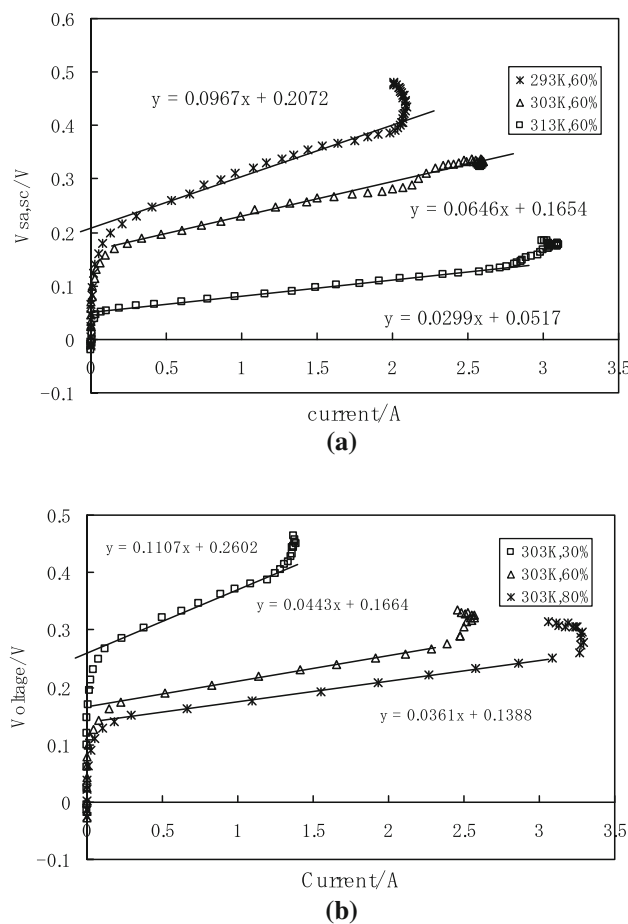
Linear plots of the current versus cathode-side boundary voltage are shown in Fig. 11. The current versus cathode-side boundary voltage for the different temperatures and different humidities are shown in Fig. 11a and b, respectively. The current exponentially increases for the cathode-side boundary voltage less than 0.3 V, as seen in Figs. 9b and 10b. The protons effectively combine with oxygen to form water at the cathode due to cathode-side boundary voltage. For the voltages greater than 0.3 to 0.7 V, the current linearly increases with the increase in the cathode-side boundary voltage as shown in Fig. 11. It suggests that the concentration of protons at the cathode is nearly proportional to the current or the supply rate of proton particles. If true, the life time of the proton particles at the cathode would be approximately constant. The saturation currents reflect Eq. 18. Therefore, the ratio of the saturation currents depends on the ratio of the values of  $(\kappa_s + 2D/L)$  and  $\rho_{so}$  for the different temperatures and different humidities, respectively. Because  $\rho_{so}$  little depends on the temperature within its range of 293 to 313 K.

Figure 12 shows the relation of current and the voltage between the two reference electrodes calculated using the measured voltages of  $V_{a,c}$ ,  $V_{a,sa}$ , and  $V_{sc,c}$ . As seen in Fig. 12, the polarization level of 0.05 to 0.25 V affects the voltage measurement at the reference electrodes in the range where no current flows. However, the voltage between the reference electrodes increases much more slowly where the current begins to flow. Therefore, the polarization would not be developed in the region in which current flows. Hence, the voltage gradient relative to the current reveals the electrical resistance of the SPE membrane. The resistance of the SPE membrane obtained in our experiment is also shown in Table 1. The calculated conductivity assuming a membrane thickness of 0.01 cm is also shown in Table 1. The resistance was calculated using



**Fig. 11** Linear plot of current versus cathode-side boundary voltage. **a** Current versus cathode-side boundary voltage for different temperatures (sample A). **b** Current versus cathode-side boundary voltage for different humidities (sample B)

the V-I measurements data made under the condition when the current flows. Therefore, the water content distribution in the element would have a gradient. The average value of the water content expressed by the extent of hydration  $\lambda (= \text{H}_2\text{O}/\text{SO}_3\text{H})$  is estimated to be about 2, 4 and 5 based on a humidity of 30, 60, and 80%, respectively.



**Fig. 12** Voltage across two reference-electrodes versus current (Voltage across the SPE membrane bulk versus current). **a** Voltage across two reference-electrodes for different temperature (sample A). **b** Voltage across two reference-electrodes for different humidities (sample B)

## 4 Discussion

### 4.1 Measurement of V–I characteristics

The V–I measurements of the dehumidifying element were done on a dehumidifying element with four electrodes in order to measure the voltage differences across the electrical double layers described in this article. From the result shown in Fig. 12, the voltages across the membrane increased to about 0.05 V or up to 0.25 V in the range in which no current flows between the main current electrodes. Therefore, polarization at the reference electrodes seems to develop in this region. However, the polarization did not develop when the current flowed. Therefore, the V–I measurements of the voltage of the reference electrodes seem to be roughly valid in the region when the current flows.

### 4.2 V–I characteristics of the anode-side double layer

Most of the applied voltage is presented on the anode-side double layer in the lower voltage range. The voltage of the cathode-side double layer is not increased in this range. In the range in which the current linearly increases, the applied voltage becomes shared with the anode-side double layer, the cathode-side double layers and the membrane. In the range where the current is saturated, the voltage across the anode-side double layer is more rapidly increased than in the range when the current linearly increases. The current can be roughly approximated by Eq. 25 as a function of the water content in the vicinity of the anode and the anode-side boundary voltage. The Gibbs energy of activation for the oxidation of water at the anode is strongly influenced by the anode-side boundary voltage.

### 4.3 V–I characteristics of the cathode-side double layer

The applied voltage is not presented on the cathode-side double layer in the range when the applied voltage is low. The voltage across the cathode-side double layer linearly increased in the range when the current linearly increased. The increasing rate decreases in the range when the current is saturated. In the middle range when the current and the voltage linearly increase, the exponent value expressed by Eq. 26 is about  $FV/(1.4-2)RT$ . This means that  $\beta_c$  is 0.5–0.7 in Eq. 12. The expression of Eq. 12 was introduced by Eq. 5, which includes  $c_o$ , the molar concentration of the oxidant. The oxidant can be protons for the cathode reaction shown in Eq. 2. Figure 11a and b shows a linear plot of  $I_{st}$  vs.  $V_{sc,c}$ . The current, or the supply rate of protons to the cathode, seems to linearly increase with the increase in the cathode-side boundary voltage in the range of more than 0.3 V up to 0.7 V. It suggested that the concentration of protons at the cathode is constant if the thickness of the cathode-side double layer remains constant.

### 4.4 Electrical resistance of SPE membrane: temperature and humidity dependences

Zawodzinski et al. measured the transport properties of Nafion 117 and reported [5] the protonic conductivity of Nafion 117 as a function of the hydration level  $\lambda (=H_2O/SO_3H)$  and temperature. The reported conductivity was about  $0.02 \text{ S cm}^{-1}$  for the temperature and hydration level of 303 K and  $\lambda = 4$ , respectively, and it roughly linearly decreased with a decrease in the water content. Anantaraman et al. also reported [6] that the conductivity of Nafion 117 is not linear with regard to the water content and that it is about  $0.002 \text{ S cm}^{-1}$  for the temperature and hydration level of 303 K and  $\lambda = 4$ , respectively. The author's results are similar to the results of Anantaraman et al. who also

measured the conductivity under the condition of a gradient water content and reported that the conductivity of Nafion 117 with a differential RH of 45%/100% is  $3.27 \times 10^{-3}$  S cm $^{-1}$ . This value is close to our results as shown in Table 1. However, the conductivity obtained by our experiments linearly changes with the change in water content, although the one by Anantaraman does not linearly change. The conductivity measurements by the authors were made under a gradient distribution of the water content by carrying the current. The membrane condition of the authors' experiments is thought to be similar to that of Anantaraman et al.

## 5 Conclusions

The measurement of the V–I characteristics of an SPE dehumidifier was made using a modified SPE dehumidifier with four electrodes which include two electrodes to carry the main current and two other reference electrodes to measure the voltage change applied to the boundary between the electrodes and membrane.

The measuring method described in this article is thought to be effective in dividing the applied voltage into the anode-side boundary voltage, the cathode-side boundary voltage and the voltage across the membrane itself.

The relation of the steady-state current and the anode-side boundary voltage was shown to be expressed in the following form.

$$I_{st} = \text{const.} \times \rho_{s,a} \times \exp\left(\frac{FV_{a,sa}}{RT}\right)$$

The steady-state current for the cathode-side boundary voltage was shown to be expressed in the following form in the region where the boundary voltage is less than 0.3 V.

$$I_{st} = \text{const.} \times \exp\left(\frac{FV_{sc,c}}{(1.4 - 2)RT}\right)$$

However, the current was saturated at more than a 0.7 V cathode-side boundary voltage.

The electric resistance of the SPE membrane (Nafion 117) itself is estimated from the differential voltage between the two reference electrodes. The estimated values are similar to the results of Anantaraman et al. [6]. The dependence of the resistance on temperature was also presented.

This method would be useful for a better understanding of the electrode phenomena in devices such as the SPE dehumidifier.

**Acknowledgements** The authors gratefully acknowledge the financial support from the Ryosai Technica Company. The authors also acknowledge Mr. Yasuda, Mr. Abe and Mr. Yamaguchi for their help with the experiments. One of the authors (S.S.) would like to thank Mr. A. Ohnuma, the former president of the Ryosai Technica Company, for providing the opportunity to carry out this study. Helpful comments from the referees are gratefully acknowledged.

## References

1. Sakuma S, Yamauchi S, Takai O (2009) J Appl Electrochem 39:815
2. Sakuma S, Yamauchi S, Takai O (2010) J Appl Electrochem 40:2153
3. Atkins P, Paula JD (2006) Physical chemistry, 8th edn
4. Yamauchi S, Mitsuda K, Maeda H, Takai O (2000) J Appl Electrochem 30:1235
5. Zawodzinski TA, D'Erouin C, Radzinski S, Sherman RJ (1993) Electrochim Soc 140(4):1041
6. Anantaraman AV, Gardner CL (1996) J Electroanal Chem 414:115